Light extinction and absorption by arbitrarily oriented finite circular cylinders by use of geometrical path statistics of rays

Min Xu

From the geometrical path statistics of rays in an anomalous-diffraction theory (ADT) [Opt. Lett. **28,** 179 (2003)] closed-form expressions for the geometrical path distribution of rays and analytical formulas for the optical efficiencies of finite circular cylinders oriented in an arbitrary direction with respect to the incident light are derived. The characteristics of the shapes of the cylinders produce unique features in the geometrical path distributions of the cylinders compared with spheroids. Gaussian ray approximations, which depend only on the mean and the mean-squared geometrical paths of rays, of the optical efficiencies of finite circular cylinders and spheroids are compared with the exact optical efficiencies in ADT. The influence of the difference in shape between cylinders and spheroids on the optical efficiencies in ADT is illustrated by their respective geometrical path distributions of rays. © 2003 Optical Society of America

OCIS codes: 290.2200, 290.4020, 290.5850, 010.1310.

1. Introduction

Light scattering by small particles has numerous applications in research into the properties of cloud and aerosol, interplanetary dust, marine environment, bacteria, and biological cells. This subject, governed by Maxwell's electromagnetic theory of light that dates to the late 19th century, was first summarized in van de Hulst's classic work[1] in 1957 and is still actively pursued, especially for nonspherical particles (see, for example, the review volume edited by Mishchenko *et al.*).[2] The availability of increased computational capability and the advance of numerical methods based on an exact theory have not decreased the attractiveness of approximate theories of light scattering in providing both simpler alternatives and much more direct physical interpretations. Approximation theories are appealing in inverse problems, such as in remote sensing in which the error introduced by the approximate theory can be negligible compared with that introduced by *a priori* assumptions. Approximation theories are sometimes also mandatory (for example, in computation of the optical efficiencies of particles of large size parameters and aspect ratios) when exact numerical methods such as the discrete dipole approximation[3,4] and the T-matrix method[5] fail because of limitations of current computational resources and in floating point accuracy.

A useful and intuitive approximation for light scattering and extinction from particles is anomalous diffraction theory (ADT).[1] It has been applied extensively to calculation of the optical efficiencies and the scattering near-forward directions of soft large particles. The requirements for ADT are that

$$|m - 1| \ll 1, \qquad x \gg 1, \tag{1}$$

where m is the complex relative refractive index and $x = 2\pi r/\lambda$ is the size parameter in which r is some characteristic dimension of the particle and λ is the wavelength of light. The first condition, $|m - 1| \ll 1$ (the so-called softness of a particle) ensures that the reflection and the refraction of the incident light by the particle can be ignored and the incident ray does not bend when it enters the particle. The second

The author (minxu@sci.ccny.cuny.edu) is with the Institute for Ultrafast Spectroscopy and Lasers, New York State Center of Advanced Technology for Ultrafast Photonic Materials and Applications, and Department of Physics, The City College and Graduate Center of the City University of New York, New York, New York, 10031.

Received 22 May 2003; revised manuscript received 5 August 2003.

0003-6935/03/336710-14$15.00/0

© 2003 Optical Society of America

condition, $x \gg 1$, ensures that the ray picture is applicable.[1,6]

The validity of the ADT has been investigated by many authors.[6–10] Farone and Robinson[7] compared the ADT result with that from exact Mie theory for a sphere. Maslowska *et al.*[9] studied the range of validity of ADT for a cube. Liu *et al.*[10] compared the ADT result with that from an exact T-matrix calculation for a finite circular cylinder and found that ADT solutions approach the rigorous T-matrix results when the refractive indices approach unity and that differences in extinction between ADT and exact solutions generally decrease with nonsphericity. Ackerman and Stephens[6] showed that the validity of the ADT improves for a polydisperse medium. More recently, the ADT was used as an aid to understanding why Mie theory overpredicts absorption and hence underpredicts the sizes of ice crystals in cirrus clouds.[11]

Exact analytical results in ADT have been obtained for only a few shapes of particles, including spheres, spheroids,[12,13] and an infinite cylinder[14] at an arbitrary orientation, and cubes,[9] a finite cylinder, and columns at some special orientations.[15] No closed-form analytical formula for optical efficiencies had been derived for a finite circular cylinder at an arbitrary orientation. Liu *et al.*[10] presented a numerical algorithm for evaluating the optical efficiencies in ADT for a finite circular cylinder at an arbitrary orientation.

Recently the ADT was shown by Xu *et al.*[16] to have a simple statistical interpretation. The optical efficiencies in ADT are determined by the probability distribution of the geometrical paths of the rays inside the particles. The main property of light extinction is characterized by the mean and the mean-squared geometrical paths of the rays, which are the basis of the Gaussian ray approximation for ADT.[16] The Gaussian ray approximation has been successfully applied for determining bacteria sizes.[17]

In this paper, this statistical point of view of anomalous diffraction extinction of light is applied to the study of the optical efficiencies of finite circular cylinders oriented in an arbitrary direction with respect to the incident light. Closed-form expressions for the geometrical path distribution of rays and analytical formulas for the optical efficiencies for such finite circular cylinders are derived for the first time to the author's knowledge. The Gaussian ray approximations, which depend only on the mean and the mean-squared geometrical paths of rays, of the optical efficiencies of finite circular cylinders and spheroids are compared with exact optical efficiencies in ADT. The differences between characteristics of shapes between cylinders and spheroids produce unique features in the geometrical path distribution. The influence of the difference in shape between cylinders and spheroids on the optical efficiencies in ADT is also discussed.

2. Theory

In the framework of ADT,[1] the extinction, absorption, and scattering efficiencies of a particle are given by

$$Q_{\text{ext}} = \frac{2}{P}\,\Re\iint_P \{1 - \exp[-ikl(m_r - 1)]\exp(-klm_i)\}\mathrm{d}P,$$
$$Q_{\text{abs}} = \frac{1}{P}\iint_P [1 - \exp(-2klm_i)]\mathrm{d}P,$$
$$Q_{\text{sca}} = Q_{\text{ext}} - Q_{\text{abs}}, \tag{2}$$

where $\Re$ represents the real part, the wave number is $k = 2\pi/\lambda$ for wavelength λ, the complex relative refractive index is $m = m_r - im_i$, l is the geometrical path of an individual ray inside the particle, and P is the projected area of the particle in the plane perpendicular to the incident light over which the integration is performed.

Our statistical approach is based on the observation that the optical efficiency in Eqs. (2) is just an average over all the geometrical paths of rays weighted by their respective contributions to the projection area. The extinction and absorption efficiencies can be written as[16]

$$Q_{\text{ext}} = 2\,\Re\int \{1 - \exp[-ikl(m_r - 1)] \times \exp(-klm_i)\}p(l)\mathrm{d}l,$$
$$Q_{\text{abs}} = \int [1 - \exp(-2klm_i)]p(l)\mathrm{d}l, \tag{3}$$

where $p(l)$ is the probability distribution function of the geometrical paths of rays inside particles and $p(l)\mathrm{d}l$ describes the probability that the geometrical path of rays inside the particles is within $[l, l + \mathrm{d}l)$.

The probability distribution function of the geometrical paths of rays (in short, the ray distribution) $p(l)$ unifies the dependence of the optical efficiencies on the nonsphericity, orientation, and polydispersity of the particle. Assume that the ray distribution for one particle with a unit size is $p_0(l)$; the ray distribution for a particle with the same shape, orientation, and a different size L is given by $p(l) = (1/L)p_0(l/L)$ from scaling of length. A system of such particles of a common shape whose sizes are distributed according to a probability-density function $n(x)$ has a ray-distribution function

$$p_{\text{pol}}(l) = \frac{\int (1/x)p_0(l/x)n(x)x^2\mathrm{d}x}{\int n(x)x^2\mathrm{d}x}, \tag{4}$$

weighted by a projection area of individual particles that is proportional to x^2. The ray distribution for a

randomly oriented particle of size L is given by a weighted average over the full 4π solid angle:

$$p_{\mathrm{rn}}(l) = \frac{\int p(l)\Sigma(\Omega)\mathrm{d}\Omega}{\int \Sigma(\Omega)\mathrm{d}\Omega}, \tag{5}$$

where $\Sigma(\Omega)$ is the projection area of the particle at orientation Ω. The subscripts pol and rn are used to denote a polydisperse particle and one that is randomly oriented, respectively.

The ray distribution for particles of even complex shapes can be computed by use of an approach similar to ray tracing. We shall examine this approach by studying the ray distribution and the optical efficiencies of arbitrarily oriented finite circular cylinders.

A. Arbitrarily Oriented Finite Circular Cylinders

Consider a finite cylinder with radius a and height L. The cylinder is bounded by side I, $z = L/2$; side II, $z = -L/2$; and side III, $x^2/a^2 + y^2/a^2 = 1$. The incident light is in the direction $\cos\chi\hat{z} + \sin\chi\hat{x}$ $(0 \le \chi < \pi/2)$. Let us rotate coordinate system xyz along the y axis for an angle χ to $x'yz'$ such that the z' axis coincides with the incident direction of light. The boundary of the cylinder is then given by

$$\begin{aligned} -x'\sin\chi + z'\cos\chi &= L/2 && \text{for side I,}\\ -x'\sin\chi + z'\cos\chi &= -L/2, && \text{for side II,}\\ \frac{(x'\cos\chi + z'\sin\chi)^2}{a^2} + \frac{y^2}{a^2} &= 1, && \text{for side III} \end{aligned} \tag{6}$$

in the new coordinate system $x'yz'$ [see Fig. (1)].

The incident beam passing through $(x', y, 0)$ on the $z' = 0$ plane intersects the boundaries of the cylinder at points $(x', y, z_{1,2}') = a(\xi\cos\chi, \eta, \zeta_{1,2})$ according to

$$\zeta_2 = \begin{cases} \dfrac{e + \xi\sin\chi\cos\chi}{\cos\chi} & |\xi + \beta| \le \sqrt{1-\eta^2} \\ \dfrac{\sqrt{1-\eta^2} - \xi\cos^2\chi}{\cos\chi} & \text{otherwise} \end{cases},$$

$$\zeta_1 = \begin{cases} \dfrac{-e + \xi\sin\chi\cos\chi}{\cos\chi} & |\xi - \beta| \le \sqrt{1-\eta^2} \\ \dfrac{-\sqrt{1-\eta^2} - \xi\cos^2\chi}{\sin\chi} & \text{otherwise} \end{cases}. \tag{7}$$

in coordinate system $x'yz'$, where $\beta \equiv L\tan\chi/2a = e\tan\chi$ and $e \equiv L/2a$. ξ and η form a set of unitless bases for the projected area of the cylinder.

Hence we obtain geometrical path l inside the cylinder:

$$l/a = \zeta_2 - \zeta_1 = \begin{cases} \dfrac{\xi + \beta + \sqrt{1-\eta^2}}{\sin\chi} & |\xi + \beta| \le \sqrt{1-\eta^2} \\ \dfrac{-\xi + \beta + \sqrt{1-\eta^2}}{\sin\chi} & |\xi - \beta| \le \sqrt{1-\eta^2} \\ \dfrac{2\sqrt{1-\eta^2}}{\sin\chi} & \text{otherwise} \end{cases} \tag{8}$$

if $\beta \ge \sqrt{1-\eta^2}$ and

$$l/a = \zeta_2 - \zeta_1 = \begin{cases} \dfrac{\xi + \beta + \sqrt{1-\eta^2}}{\sin\chi} & -\sqrt{1-\eta^2} - \beta \le \xi \le -\sqrt{1-\eta^2} + \beta \\ 2e/\cos\chi & -\sqrt{1-\eta^2} + \beta \le \xi \le \sqrt{1-\eta^2} - \beta \\ \dfrac{-\xi + \beta + \sqrt{1-\eta^2}}{\sin\chi} & \sqrt{1-\eta^2} - \beta \le \xi \le \sqrt{1-\eta^2} + \beta \\ \dfrac{2\sqrt{1-\eta^2}}{\sin\chi} & \text{otherwise} \end{cases} \tag{9}$$

if $\beta < \sqrt{1-\eta^2}$.

The projected area of the cylinder is the area formed by the points of tangency ($l = 0$) on the $z' = 0$ plane. This area is enclosed inside $\eta = \pm 1$ and $(\xi \pm \beta)^2 + \eta^2 = 1$ when Eqs. (8) and (9) are equated to zero and hence is given by (see Fig. 2)

$$\Sigma = 2aL\sin\chi + \pi a^2\cos\chi = 4a^2\cos\chi[\beta + (\pi/4)]. \tag{10}$$

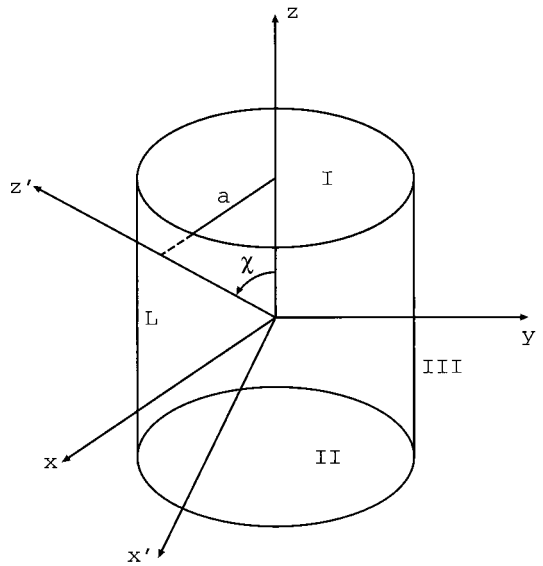

Fig. 1. Finite circular cylinder bounded by sides I, II, and III. The revolutional axis of the cylinder makes angle χ with the incident beam.

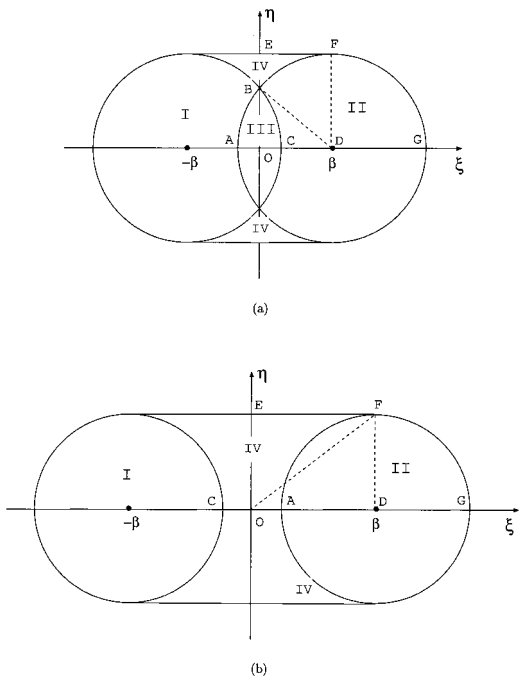

Fig. 2. Projected area of a cylinder whose revolutional axis makes angle χ with the incident light: (a) $\beta < 1$, (b) $\beta \geq 1$.

Geometrical path l in Eqs. (8) and (9) can be rewritten as

$$t \equiv \frac{l \sin \chi}{a} = (\zeta_2 - \zeta_1)\sin \chi = \begin{cases} \xi + \beta + \sqrt{1 - \eta^2} & \text{in I} \\ -\xi + \beta + \sqrt{1 - \eta^2} & \text{in II} \\ 2\beta & \text{in III} \\ 2\sqrt{1 - \eta^2} & \text{in IV} \end{cases} \tag{11}$$

inside regions I, II, III, and IV of the projected area as specified in Fig. 2 where region III is absent for $\beta \geq 1$. The quantity t defined in Eq. (11) will henceforth be called the scaled geometrical path.

Because of the symmetry presented here, we need to consider only the first quadrant in Fig. 2 in the calculation of the geometrical path distribution of rays for the cylinder. Distribution function $p(l)$ of the geometrical paths of rays is proportional to the total area density $q(t)$ inside the first quadrant. Here $q(t)\mathrm{d}t$ describes the area inside the first quadrant through which the scaled geometrical path of rays is within $[t, t + \mathrm{d}t)$. After a straightforward computation [see Appendix A for details], we find that

$$q(t) = \begin{cases} \left\{ \dfrac{\sqrt{4 - t^2}}{2} + \dfrac{(t/2)[\beta - (t/2)]}{\sqrt{4 - t^2}} \right\} H(2\beta - t) + \dfrac{\arccos \beta - \beta\sqrt{1 - \beta^2}}{2}\, \delta(t - 2\beta) & \beta < 1 \\ \left\{ \dfrac{\sqrt{4 - t^2}}{2} + \dfrac{(t/2)[\beta - (t/2)]}{\sqrt{4 - t^2}} \right\} H(2 - t) & \beta \geq 1 \end{cases}, \tag{12}$$

where $H(x) = 1$ if $x > 0$ and $H(x) = 0$ otherwise is the Heaviside function and $\delta(x)$ is the Dirac delta function. Equation (12) satisfies

$$\int_0^{+\infty} q(t)\mathrm{d}t = \beta + (\pi/4), \tag{13}$$

yielding the projected area inside the first quadrant on the $\xi\eta$ plane, as expected. The geometrical path distribution of rays for a finite cylinder whose revolution axis forms an angle χ with the incident light is given by

$$p(l) = \frac{\sin \chi q(l/\sin \chi/a)}{\alpha\beta + (\pi/4)}. \tag{14}$$

We obtain the exact optical efficiencies of the cylinder in ADT by plugging distribution function (14) into (3). Introducing absorption angle α,

$$\tan \alpha = \frac{m_i}{m_r - 1}, \tag{15}$$

and phase shift

$$\rho^* = \rho(1 - i \tan \alpha), \tag{16}$$

with a real parameter

$$\rho = \frac{2ka(m_r - 1)}{\sin \chi}, \tag{17}$$

yields for the extinction efficiency

$$Q_{\text{ext}} = \begin{cases} 2 - \dfrac{4}{\beta + (\pi/4)} \Re\left[G(\rho^*; \arcsin \beta) + \dfrac{\arccos \beta - \beta\sqrt{1 - \beta^2}}{4} \exp(-i\rho^*\beta) \right] & \beta < 1 \\ 2 - \dfrac{4}{\beta + (\pi/4)} \Re G(\rho^*; \pi/2) & \beta \geq 1 \end{cases}, \tag{18}$$

where the function G is defined as

$$\begin{aligned} G(u; \phi) &= \int_0^\phi \exp(-iu \sin \theta)\left(\frac{3}{2}\cos^2 \theta - \frac{1}{2} + \frac{\beta}{2}\sin \theta\right) d\theta \\ &= \frac{3}{2}\frac{1 - \cos \phi \exp(-iu \sin \phi)}{iu} - \frac{1}{2} \\ &\quad \times \int_0^\phi \exp(-iu \sin \theta) d\theta + \frac{1}{2}\left(\beta - \frac{3}{iu}\right) \\ &\quad \times \int_0^\phi \exp(-iu \sin \theta) \sin \theta d\theta. \end{aligned} \tag{19}$$

In particular,

$$\begin{aligned} G\left(u; \frac{\pi}{2}\right) &= \frac{\beta}{2} - \frac{\pi}{4}[J_0(u) - i\mathbf{H}_0(u)] - \frac{\pi}{4}\left(\beta + i\frac{3}{u}\right) \\ &\quad \times [\mathbf{H}_1(u) + iJ_1(u)], \end{aligned} \tag{20}$$

where J_0 and J_1 are the zeroth- and first-order Bessel functions and $\mathbf{H}_0$ and $\mathbf{H}_1$ are the zeroth- and first-order Struve functions, respectively.

The absorption efficiency for the cylinder is expressed as

$$Q_{\text{abs}} = \left\{ \begin{array}{ll} 1 - \dfrac{2}{\beta + (\pi/4)}\left[G(-i2\rho \tan \alpha; \arcsin \beta) + \dfrac{\arccos \beta - \beta\sqrt{1 - \beta^2}}{4} \exp(-2\rho\beta \tan \alpha) \right] & \beta < 1 \\ 1 - \dfrac{2}{\beta + (\pi/4)} G(-i2\rho \tan \alpha; \pi/2) & \beta \geq 1 \end{array} \right\}. \tag{21}$$

Some special cases of the extinction and absorption efficiencies of a cylinder are in order. When the phase delay of the central ray is large ($\rho \to \infty$), the extinction efficiency in Eq. (18) reduces to $Q_{\text{ext}} \to 2$, and the absorption efficiency in Eq. (21) reduces to $Q_{\text{abs}} \to 0$ if the absorption angle is $\alpha \neq 0$, as expected. When the phase delay of the central ray is small ($\rho \to 0$), the extinction and absorption efficiencies reduce to

$$\begin{aligned} Q_{\text{ext}} &= 2km_i\langle l\rangle + k^2[(m_r - 1)^2 - m_i^2]\langle l^2\rangle, \\ Q_{\text{abs}} &= 2km_i\langle l\rangle - 2k^2 m_i^2\langle l^2\rangle, \end{aligned} \tag{22}$$

where the mean and the mean-squared geometrical paths are given by Eqs. (35) and (36) below by expansion of Eqs. (18) and (21) and omission of the terms that decay faster than ρ^2.

When angle $\chi = 0$, the ray distribution is given simply by $p(l, \chi = 0) = \delta(l - L)$, and the extinction and absorption efficiencies are given by

$$\begin{aligned} Q_{\text{ext}}(\chi = 0) &= 2 - 2\cos[kL(m_r - 1)]\exp(-kLm_i), \\ Q_{\text{abs}}(\chi = 0) &= 1 - \exp(-2kLm_i). \end{aligned} \tag{23}$$

When angle $\chi = \pi/2$, the ray distribution is $p(l, \chi = \pi/2) = lH(2a - l)/2a\sqrt{4a^2 - l^2}$, and the extinction and absorption efficiencies are given by

$$\begin{aligned} Q_{\text{ext}}\left(\chi = \frac{\pi}{2}\right) &= \pi\, \Re[\mathbf{H}_1(\rho^*) + iJ_1(\rho^*)], \\ Q_{\text{abs}}\left(\chi = \frac{\pi}{2}\right) &= \frac{\pi}{2}[I_1(2\rho \tan \alpha) - \mathbf{L}_1(2\rho \tan \alpha)], \end{aligned} \tag{24}$$

where I_1 is the first-order modified Bessel function and $\mathbf{L}_1$ is the first-order modified Struve function. In the absorptionless case the extinction efficiency reduces to the well-known result that $Q_{\text{ext}}(\chi = \pi/2) = \pi\mathbf{H}_1(\rho)$.[1]

The extinction and absorption efficiencies of the disklike cylinder ($e \equiv L/2a \to 0$) and the needlelike cylinder ($e \to \infty$) at an arbitrary orientation χ are found to take the same forms as Eqs. (23) and (24), respectively, that originate from their geometrical similarities. In the former case, length L in Eqs. (23) needs to be replaced by $L/\cos \chi$.

B. Randomly Oriented Finite Circular Cylinders

The geometrical path distribution for a randomly oriented cylinder is obtained from

$$p_{\mathrm{rn}}(l) = \frac{\displaystyle\int_0^{\pi/2} \mathrm{d}\chi\, \frac{1}{a} \sin^2\chi \cos\chi q\left(\frac{l}{a}\sin\chi\right)}{\displaystyle\int_0^{\pi/2} \mathrm{d}\chi \sin\chi \cos\chi[e \tan\chi + (\pi/4)]} \tag{25}$$

weighted by the projection area given in Eq. (10) of the particle oriented at angle χ with respect to the incident light.

The geometrical path distribution for a randomly oriented cylinder is found to be

$$\begin{aligned} p_{\mathrm{rn}}(l) = \frac{1}{(\pi/8)(1+2e)a} \Bigg(& H(e-x)D(\arctan e^{-1}, x) \\ & + H(x-e)H(\sqrt{e^2+1}-x) \\ & \times \left[D(\arctan e^{-1}, x) - D\left(\arccos\frac{e}{x}, x\right)\right] \\ & + H(1-x)\left[D\left(\frac{\pi}{2}, x\right) - D(\arctan e^{-1}, x)\right] \\ & + H(x-1)H(\sqrt{e^2+1}-x)\Big[D(\arcsin x^{-1}, x) \\ & - D(\arctan e^{-1}, x)] + H(x-e)H(\sqrt{e^2+1} \\ & - x)\frac{e^2}{4x^3}\{\arccos\sqrt{x^2-e^2} - [(x^2-e^2)(1+e^2 \\ & - x^2)]^{1/2}\}\Bigg), \end{aligned} \tag{26}$$

in which $x \equiv l/2a$ and function $D(\chi, x)$ is defined as

$$\begin{aligned} D(\chi, x) &= \int \mathrm{d}\chi \sin^2\chi \cos\chi\left[\Delta + \frac{x\sin\chi(e\tan\chi - x\sin\chi)}{2\Delta}\right] \\ &= \frac{6x^2\sin^2\chi + 1}{16x^2}\sin\chi\Delta - \frac{1}{16x^3}\arcsin(x\sin\chi) + \frac{e\sin\chi\cos\chi\Delta}{6x} \\ &\quad + \frac{e(2+x^2)}{6x^3}F(\chi, x) - \frac{e(1+x^2)}{3x^3}E(\chi, x), \end{aligned}$$

where $\Delta \equiv (1 - x^2\sin^2\chi)^{1/2}$ and $F(\chi, x)$ and $E(\chi, x)$ are elliptic integrals of the first and second kinds:

$$\begin{aligned} F(\chi, x) &= \int_0^{\chi} \frac{\mathrm{d}a}{(1 - x^2\sin^2 a)^{1/2}}, \\ E(\chi, x) &= \int_0^{\chi} (1 - x^2\sin^2 a)^{1/2}\mathrm{d}a. \end{aligned} \tag{27}$$

We obtain the optical efficiencies by plugging Eq. (26) into Eqs. (3).

C. Probability Density of Zero Geometrical Paths

One important property of the ray distribution of cylinders is the nonzeroness of the probability density of zero geometrical paths that originates from the sharp edges of cylinders. This probability density of zero paths for a finite cylinder oriented at an angle χ with respect to the incident light is given by

$$p(0) = \frac{\sin\chi}{a(\beta + \pi/4)}. \tag{28}$$

The probability density of zero paths becomes

$$p_{\mathrm{rn}}(0) = \frac{8}{3\pi(a+L)} \tag{29}$$

for a randomly oriented finite circular cylinder.

The geometrical path distribution of polydisperse finite circular cylinders is related to the ray distribution of monosized particles through Eq. (4). The probability density of zero paths of polydisperse particles is expressed simply as

$$p_{\mathrm{pol}}(0) = p(0)\exp(-3\sigma^2/2), \tag{30}$$

$$p_{\mathrm{pol,rn}}(0) = p_{\mathrm{rn}}(0)\exp(-3\sigma^2/2) \tag{31}$$

for fixed and randomly oriented polydisperse particles with a log-normal distribution[18] given by

$$n(r) = \frac{1}{(2\pi)^{1/2}\sigma} r^{-1} \exp\left[-\frac{\ln^2(r/a_m)}{2\sigma^2}\right], \tag{32}$$

normalized to $\int_0^{\infty} n(r)\mathrm{d}r = 1$, where r is the characteristic size of the particle. Here $p(0)$ and $p_{\mathrm{rn}}(0)$ are the probability densities of zero paths for monosized particles of size a_m.

D. Mean and Mean-Squared Geometrical Paths and Gaussian Ray Approximation

The averaging over the orientations and the polydispersity of the particle tend to wash out the shape characteristics of an individual particle. Ray distribution $p(l)$ for a system of polydisperse and randomly oriented particles such as a bacteria suspension is characterized essentially by the mean geometrical path $\langle l\rangle = \int lp(l)\mathrm{d}l$ and the mean-squared geometrical path $\langle l^2\rangle = \int l^2 p(l)\mathrm{d}l$ of rays inside the particles. This ray distribution approaches a Gaussian ray distribution:

$$\begin{aligned} p^{\mathrm{Gau}}(x) &= \frac{1}{\sqrt{2\pi}v}\exp\left[-\frac{(x-\mu)^2}{2\nu^2}\right], \\ \mu &= \langle l\rangle, \quad \nu = \sqrt{\langle l^2\rangle - \langle l\rangle^2}, \end{aligned} \tag{33}$$

with the extinction and absorption efficiencies in the Gaussian ray approximation[16] given by

$$Q_{\text{ext}}^{\text{Gau}} = 2 - 2\cos[k(m_r - 1)(\mu - k\nu^2 m_i)]\exp\left\{-k\mu m_i - \frac{k^2\nu^2[(m_r-1)^2 - m_i^2]}{2}\right\},$$

$$Q_{\text{abs}}^{\text{Gau}} = 1 - \exp[-2km_i(\mu - k\nu^2 m_i)] \tag{34}$$

from Eqs. (3).

The mean and the mean-squared geometrical paths of rays can easily be obtained from the geometrical path distribution of rays. The mean and the mean-squared geometrical paths for a cylinder oriented at an angle χ are given by

$$\langle l\rangle = \frac{a}{\sin\chi}\frac{\pi\beta}{2[\beta + (\pi/4)]}, \tag{35}$$

$$\langle l^2\rangle = \begin{cases} \dfrac{a^2}{\sin^2\chi}\dfrac{1}{\beta + (\pi/4)}\left[\dfrac{8}{3}\beta - \dfrac{\pi}{4} + \dfrac{1}{2}(1 + 4\beta^2)\arccos\beta - \dfrac{1}{6}\beta(2\beta^2 + 13)\sqrt{1-\beta^2}\right] & \beta < 1 \\ \dfrac{a^2}{\sin^2\chi}\dfrac{(8/3)\beta - (\pi/4)}{\beta + (\pi/4)} & \beta \geq 1 \end{cases}, \tag{36}$$

respectively, from Eq. (14).

The mean and the mean-squared geometrical paths for a randomly oriented finite cylinder are an average over all the orientation angles weighted by their projection areas:

$$\langle l\rangle_{\text{rn}} = \frac{\int_0^{\pi/2} d\chi \sin\chi\langle l\rangle\cos\chi[\beta + (\pi/4)]}{\int_0^{\pi/2} d\chi \sin\chi\cos\chi[\beta + (\pi/4)]} = \frac{4e}{1 + 2e}a, \tag{37}$$

$$\begin{aligned}\langle l^2\rangle_{\text{rn}} &= \frac{\int_0^{\pi/2} d\chi \sin\chi\langle l^2\rangle\cos\chi[\beta + (\pi/4)]}{\int_0^{\pi/2} d\chi \sin\chi\cos\chi[\beta + (\pi/4)]} \\ &= \frac{8a^2e^2}{2e+1}\left\{\frac{4}{3e} + \frac{e}{6(e + \sqrt{e^2+1})} - \frac{13\sqrt{e^2+1}}{12e} + 1 + \ln\frac{e + \sqrt{e^2+1}}{2e} - \frac{1}{4e^2}\ln(e + \sqrt{e^2+1})\right\} \\ &= \frac{8a^2e^2}{2e+1}\begin{cases} (4/3)e^{-1} - (1/4)[\ln 2e + (5/4)]e^{-2} - \dfrac{1}{96}e^{-4} + \dfrac{1}{768}e^{-6} + \mathcal{O}(e^{-7}) & e \to \infty \\ \ln(1/e) + 1 - \ln 2 + (2/3)e - (1/6)e^2 + (1/30)e^3 - (1/420)e^5 + \mathcal{O}(e^6) & e \to 0 \end{cases}\end{aligned} \tag{38}$$

respectively. Note that the aspect ratio $e \equiv \epsilon^{-1}$. The mean geometrical path is $\langle l\rangle_{\text{rn}} = V/\langle\Sigma\rangle_{\text{rn}}$, where V is the volume of the particle, $\langle\Sigma\rangle$ is the mean geometrical projection area of the particle, and $\langle\Sigma\rangle_{\text{rn}} = S/4$ for a randomly oriented convex particle whose surface area is S.

The mean and the mean-squared ray paths of a polydisperse particle relate simply to those of a monosized particle by

$$\langle l\rangle_{\text{pol}} = \langle l\rangle_0 \exp(5\sigma^2/2), \tag{39}$$

$$\langle l^2\rangle_{\text{pol}} = \langle l^2\rangle_0 \exp(6\sigma^2), \tag{40}$$

where the polydisperse particle has a log-normal particle size distribution [Eq. (32)] characterized by a_m and σ, and $\langle\ \rangle_0$ is the corresponding value of a monosized particle of size a_m.

The geometrical path statistics of rays provide a standardized procedure for evaluating optical efficiencies in ADT. The derivation of the ray distribu-

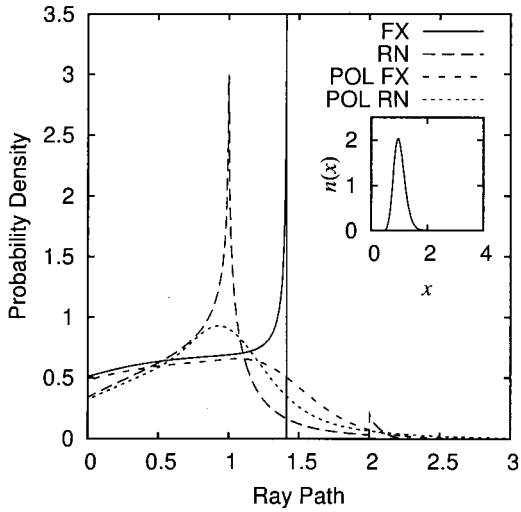

(a)

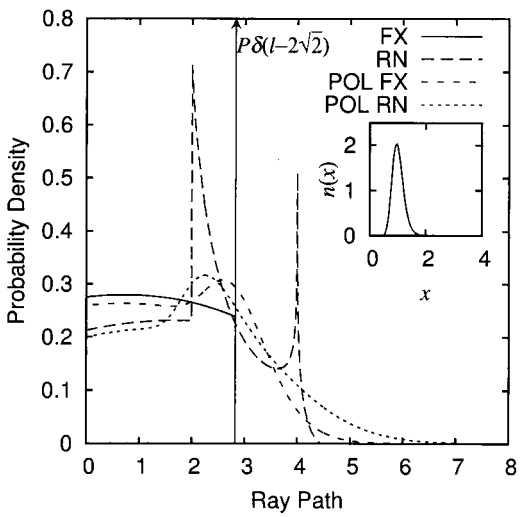

(b)

Fig. 3. Ray distributions for a finite circular cylinder at a fixed orientation $\chi = \pi/4$ (FX), randomly oriented (RN), polydisperse at a fixed orientation $\chi = \pi/4$ (POL FX), and randomly oriented polydisperse (POL RN). Axial ratio of the cylinder: (a) $\epsilon = 0.5$, (b) $\epsilon = 2$. Height of the cylinder, $L = 2$ for the monosized cylinder. The log-normal size distribution $n(x)$ of the half-height $(L/2)$ of the polydisperse cylinder with $a_m = 1$ and $\sigma = 0.2$ is also as insets. The height of the delta-function peak in (b) for the monosized cylinder at a fixed orientation is $P = (4\pi - 3\sqrt{3})/6(\pi + 2) \simeq 0.239$.

tion for a spheroid is given in Appendix B. Appendix C lists the geometrical cross sections, mean and mean-squared root paths of spheres, and randomly oriented spheroids and cylinders.

3. Results and Discussion

A. Ray Distributions of Cylinders and Spheroids

The ray distributions from a finite circular cylinder, a randomly oriented cylinder, a system of polydisperse cylinders at a fixed orientation, and a system of randomly oriented polydisperse cylinders are plotted in Fig. 3. Figures 3(a) and 3(b) show the ray distributions for cylinders of axial ratios $\epsilon = 0.5$ and $\epsilon = 2$, respectively. The ray distribution for a monosized cylinder at a fixed orientation (solid curves in Fig. 3) is nearly flat, except for a peak at the largest value of the ray path. The peak is a delta function for a cylinder that satisfies $\beta = \epsilon^{-1} \tan \chi < 1$, originating from the second term in Eq. (12), where the rays intersect with sides I and II of the cylinder [Fig. 3(b)]. Two peaks occur, at the values of the ray path of the diameter $2a$ and the height L of the cylinder, for the ray distribution of randomly oriented monosized cylinders (long-dashed curves in Fig. 3. The ray distribution for a polydisperse finite circular cylinder, either at a fixed orientation (dashed curves lines in Fig. 3) or randomly oriented (short-dashed curves in Fig. 3), pertains to a smooth bell shape whose left wing is pushed up for an amount specified in Eqs. (30) and (31). This probability density of zero geometrical paths approaches zero with the increase of the dispersion σ of the particle size distribution of the cylinder.

The ray distributions for spheroids with axial ratios $\epsilon = 0.5$ and $\epsilon = 2$ are plotted in Fig. 4. The ray distribution for a spheroid at a fixed orientation (solid curves in Fig. 4) is triangular. One peak occurs at the value of the ray path of the shorter diameter $2a$ of the spheroid for the ray distribution of randomly oriented monosized spheroids (long-dashed curves in Fig. 4). The ray distribution for a polydisperse spheroid, either at a fixed orientation (dashed curves lines in Fig. 4) or randomly oriented (short-dashed curves in Fig. 4), has a smooth bell shape. One significant feature of the ray distribution of spheroids is the zero probability density of a zero ray path.

The different characteristics of the shapes of cylinders and spheroids produce unique features in the geometrical path distribution. One significant difference between a cylinder and a spheroid is the presence of the appreciable nonzero probability density of zero ray paths for the cylinder owing to its sharp edges, whereas the probability density of zero ray paths for spheroids is always zero.

The ray distribution for a randomly oriented cylinder has two peaks, located at its diameter $2a$ and its height L. By contrast, only one peak appears in the ray distribution for a randomly oriented spheroid at the length of its shorter axis. The second peak in the ray distribution of the cylinder diminishes with a decrease in the aspect ratio, yielding a ray distribution more like that of spheroid than of a cylinder.

B. Mean and Mean-Square-Root Paths of Cylinders and Spheroids

Figure 5 plots the mean and the mean-square-root geometrical paths for a randomly oriented cylinder and a spheroid. The cylinder and the spheroid are of a common aspect ratio ϵ and of a common surface area equal to that of a sphere of radius a_s. The mean and the mean-square-root ray paths of the spheroid are larger than those of the cylinder when the aspect ratio is ~ 1. The situation is reversed in the limits of

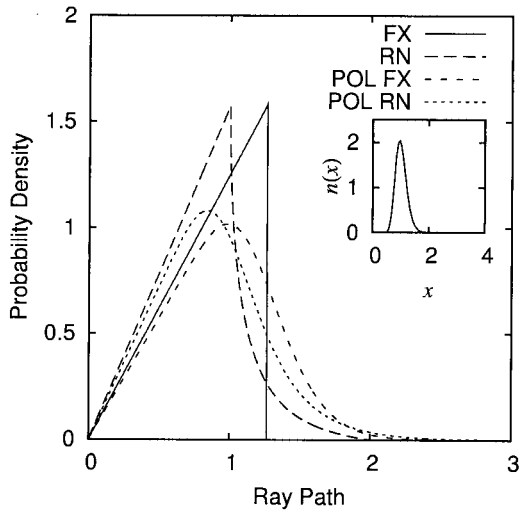

(a)

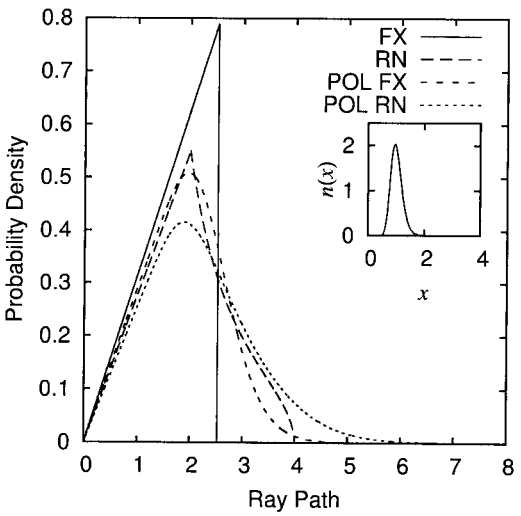

(b)

Fig. 4. Ray distributions for a spheroid at a fixed orientation $\chi = \pi/4$ (FX), randomly oriented (RN), polydisperse at a fixed orientation (POL FX), and randomly oriented polydisperse (POL RN). Axial ratio of the spheroid: (a) $\epsilon = 0.5$, (b) $\epsilon = 2$. The semisize of the revolutional axis of the monosized spheroid is 1. Log normal-size distribution $n(x)$ with $a_m = 1$ and $\sigma = 0.2$ for the semisize of the revolutional axis of the spheroid is plotted as insets.

both small and large aspect ratios. The difference between the mean and the mean-square-root ray paths of the cylinder and of the spheroid tends to be negligible for small aspect ratios (needlelike) but is significant for large aspect ratios (disklike). This result is consistent with the observation that the second peak in the ray distribution of a randomly oriented cylinder diminishes with decreasing aspect ratio and more closely resembles that of the spheroid.

Figure 6 plots the ratio of the ray path dispersion to the mean geometrical path for cylinders and spheroids. Near the region of a unity aspect ratio, this ratio for spheroids is much less than that of cylinders,

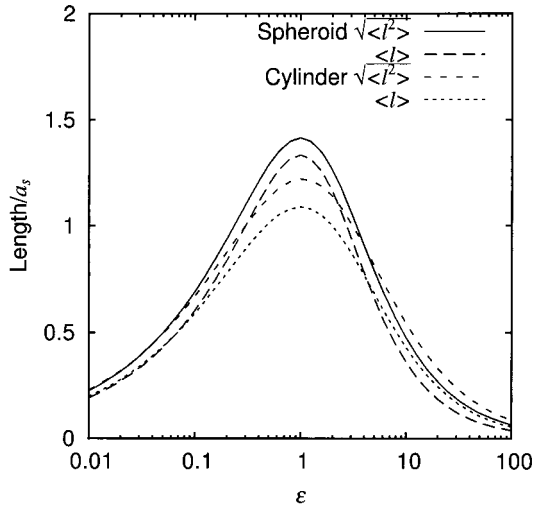

Fig. 5. Mean and mean-square-root geometrical paths for a randomly oriented cylinder and spheroid with a common aspect ratio ϵ and a common surface areas of a sphere of radius a_s.

as the spheroid has a smaller dispersion in the geometrical ray paths than does the cylinder.

C. Performance of the Gaussian Ray Approximation and Difference in Optical Efficiencies between Cylinders and Spheroids

Both random orientation and polydispersity of a particle tend to smear the characteristic features of the ray distribution of the particle. The ray distributions of the polydisperse cylinder and the spheroid, either randomly oriented or not, approach a bell shape. The characteristic features of the ray distribution of a particle are gradually washed out (see Figs. 3 and 4). The main feature of the ray distribution is captured by its mean and its mean-square-root geometrical paths.

Thus the Gaussian ray approximation, which de-

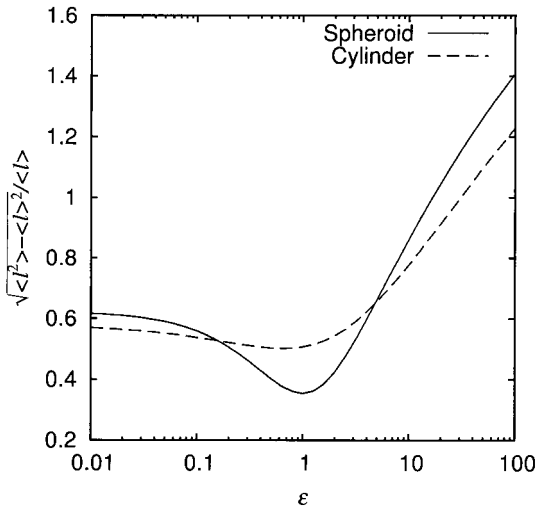

Fig. 6. Ratio of the ray path dispersion over mean geometrical paths for cylinders and spheroids.

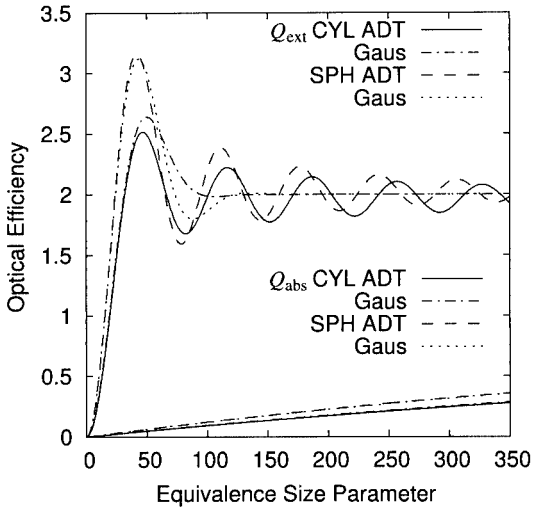

(a)

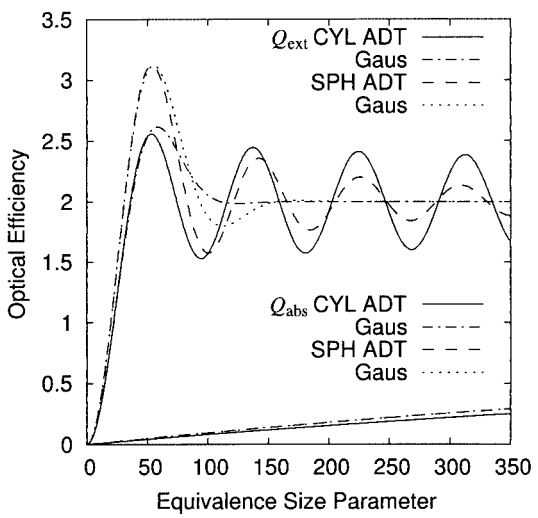

(b)

Fig. 7. Extinction and absorption efficiencies of cylinders (CYL) and spheroids (SPH) with aspect ratios (a) $\epsilon = 0.5$ and (b) $\epsilon = 2$. The equivalence size parameter is the size parameter of the sphere whose surface area is the same as that of the cylinder and the spheroid. Both the cylinder and the spheroid are oriented at a fixed orientation $\chi = \pi/4$. Relative refractive index of both cylinders and spheroids, $m = 1.05 - i0.0005$.

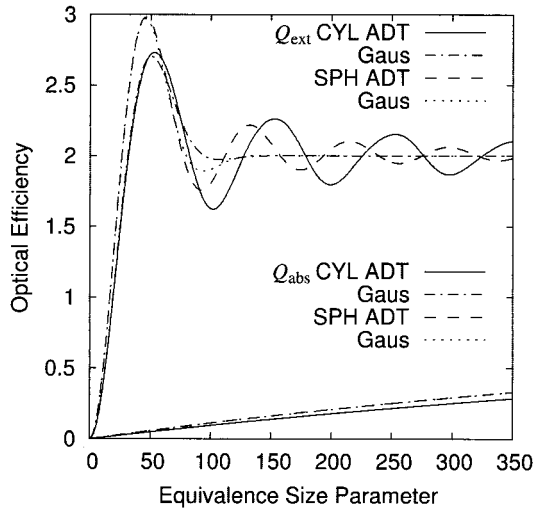

(a)

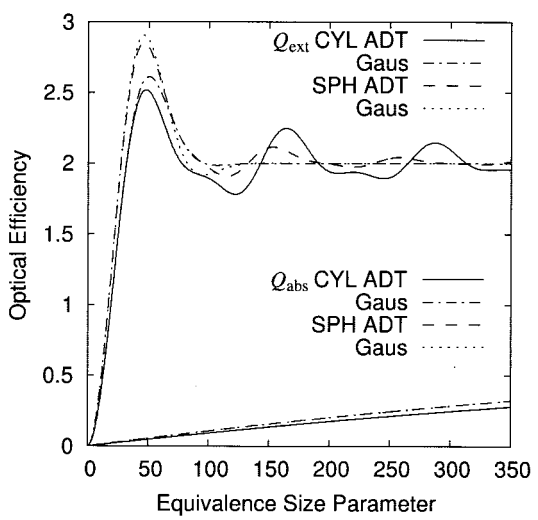

(b)

Fig. 8. Extinction and absorption efficiencies of cylinders (CYL) and spheroids (SPH) with aspect ratios (a) $\epsilon = 0.5$ and (b) $\epsilon = 2$. Both the cylinder and the spheroid are randomly oriented.

pends only on the mean and the mean-square-root geometrical paths, becomes a good approximation for anomalous light diffraction for polydisperse or randomly oriented particles or both. Figures 7, 8, 9, and 10 plot the optical efficiencies of cylinders and spheroids with a common surface area and with aspect ratios $\epsilon = 0.5$ and $\epsilon = 2$ for cases with fixed orientation, with random orientation, polydisperse and with fixed orientation, and polydisperse and randomly oriented, respectively. The relative refractive index of cylinders and spheroids is $m = 1.05 - i0.0005$.

The Gaussian ray approximation reduces to the exact ADT in limits of both small and large size parameters of the particle. The maximum relative error of the absorption efficiency of the Gaussian ray approximation (Gaus) compared with the exact ADT is less than 0.3% for the cylinders in Figs. 7–10, except for the cylinder with aspect ratio $\epsilon = 0.5$ and fixed in orientation $\chi = \pi/4$, whose maximum relative error equals 3.1% (Fig. 7). The maximum relative error of the absorption efficiency is less than 0.07% for the spheroids in Figs. 7–9 and ~0.25% in Fig. 10 for the polydisperse and randomly oriented spheroids.

The maximum relative error of the extinction efficiency is ~35% for the monosized cylinder fixed in orientation $\chi = \pi/4$ in Fig. 7 and reduces progressively to less than 8% for the polydisperse and random oriented cylinder in Fig. 10. The maximum relative error of the extinction efficiency of the spheroid is ~25% when the spheroid is fixed in an orien-

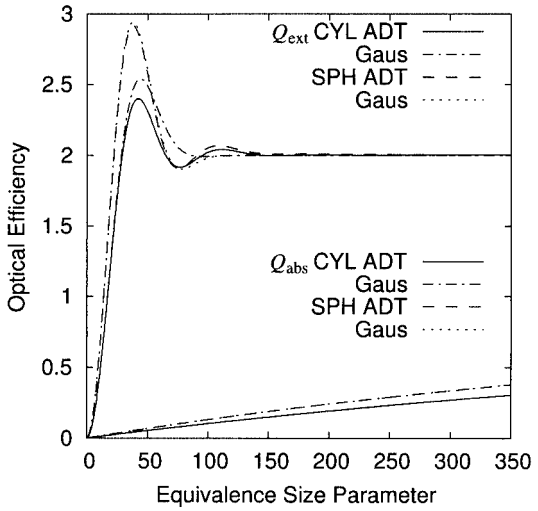

(a)

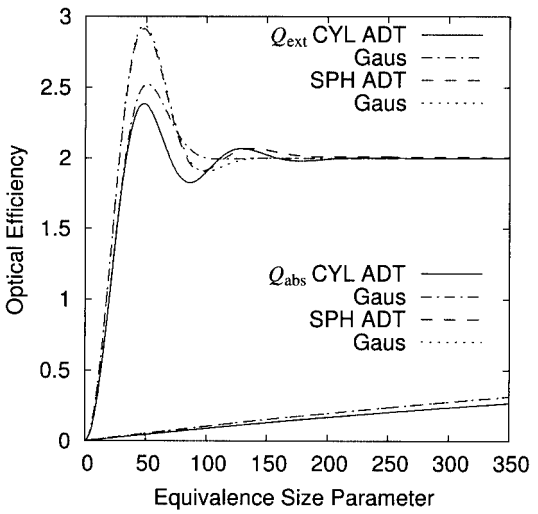

(b)

Fig. 9. Extinction and absorption efficiencies of cylinders (CYL) and spheroids (SPH) with aspect ratios (a) $\epsilon = 0.5$ and (b) $\epsilon = 2$. The equivalence size parameter is the size parameter of the sphere of an equivalent surface area of the respective particle of size a_m. The dispersion of the log-normal size distribution of the cylinder and the spheroid is $\sigma = 0.2$. Both the cylinder and the spheroid are polydisperse and oriented at a fixed orientation $\chi = \pi/4$.

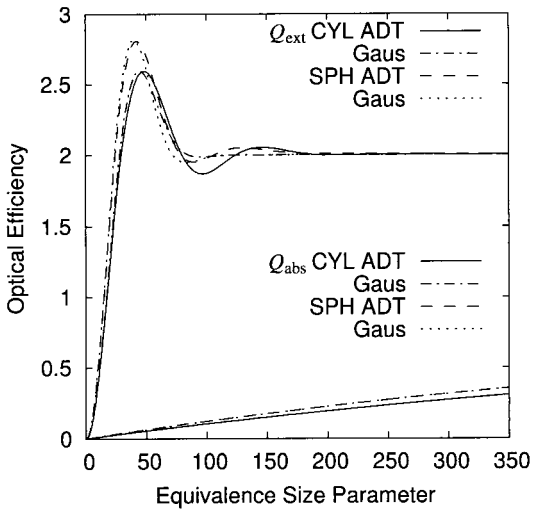

(a)

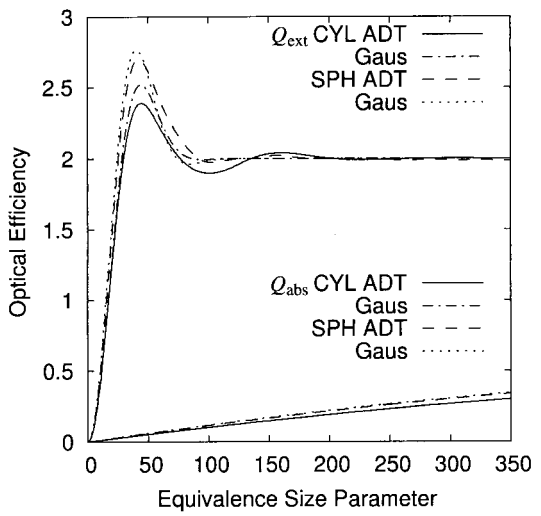

(b)

Fig. 10. Extinction and absorption efficiencies of cylinders (CYL) and spheroids (SPH) with aspect ratios (a) $\epsilon = 0.5$ and (b) $\epsilon = 2$. Both the cylinder and the spheroid are polydisperse and randomly oriented.

tation of $\chi = \pi/4$. The maximum relative error reduces to less than 4% for the monosized and randomly oriented spheroid. This value becomes ~8% for the polydisperse and randomly oriented spheroids. The abnormal increase of error in the Gaussian ray approximation for a polydisperse and randomly oriented spheroid compared with that for a monosized randomly oriented spheroid reflects the fact that the ray distribution of the latter is closer to a Gaussian distribution. This means that excessive polydispersion may occasionally degrade the accuracy of the Gaussian ray approximation of anomalous light diffraction.

Some comparisons of the optical efficiencies of cylinders and spheroids are in order. The Gaussian approximation works extremely well for the absorption efficiency of both cylinders and spheroids. For the extinction efficiency, the Gaussian ray approximation works better for spheroids than for cylinders. This result can be attributed to the appreciable nonzero probability density of zero ray paths for the cylinder (the left wing of the bell shape of the ray distribution is pushed up). For the aspect ratios $\epsilon = 0.5$ and $\epsilon = 2$ plotted in Figs. 7–10, the absorption efficiency of the spheroids is larger than that of the cylinders, mainly because of a larger mean geometrical path of rays for spheroids in that region of aspect ratios (see Fig. 5). The same fact also explains the reason that first peak of

the extinction curve of the spheroid is higher than that of the cylinder.

The periodic structure of extinction curves is linked closely to the peaks presented in the ray distribution of the particles. One sharp peak in the ray distribution produces a train of exponentially decaying sinusoidal peaks in the extinction curve whose spacing is inversely proportional to the positioning of the peak in the ray distribution. This is most evident in Fig. 8(b), where the extinction curve exhibits the composite of two trains of exponentially decaying sinusoidal peaks that originated from the two peaks presented in its ray distribution of the randomly oriented cylinder of aspect ratio $\epsilon = 2$.

In conclusion, I have demonstrated a geometrical path statistical approach to anomalous light diffraction. The exact closed-form analytical geometrical path distribution and the optical efficiencies of finite circular cylinders oriented in an arbitrary direction with respect to the incident light have been derived. The different characteristics of the shapes of cylinders and spheroids produce unique features in their geometrical path distributions, including the nonzero probability density of zero ray paths for cylinders versus the zero probability density of zero ray paths for spheroids and different numbers of peaks present at characteristic lengths for randomly oriented cylinders and spheroids. The Gaussian ray approximations, which depend only on the mean and the mean-squared geometrical paths of rays, of the optical efficiencies of finite circular cylinders and spheroids are then compared with the exact optical efficiencies of the ADT. The influence of the shape difference of cylinders and spheroids on the optical efficiencies in the ADT is illustrated by their respective ray distributions.

Appendix A: Area Density in the First Quadrant

Total area density $q(t)$ is the sum of area densities $q_i(t)$ from regions $i = 2, 3, 4$ if $\beta < 1$ or $i = 2, 4$ if $\beta \geq 1$. Let us consider region II of Fig. 2 first. We denote $\xi = \beta + \rho \cos \theta$ and $\eta = \rho \sin \theta$; azimuthal angle θ for a geometrical path of length t inside region II in Eq. (11) can be solved as

$$\cos \theta = \frac{1 - t^2 - \rho^2}{2t\rho}, \qquad 0 \leq \rho \leq 1, \quad 1 - \rho \leq t \leq 1 + \rho. \tag{A1}$$

Hence the area in region II with a geometrical path of length within $[t, t + \mathrm{d}t]$ is given by

$$\int \rho \mathrm{d}\rho \mathrm{d}\theta = q_2(t)\mathrm{d}t = \mathrm{d}t \times \int \mathrm{d}\rho \, \frac{\rho(1 + t^2 - \rho^2)}{t[-\rho^4 + 2(t^2 + 1)\rho^2 - (t^2 - 1)^2]^{1/2}}. \tag{A2}$$

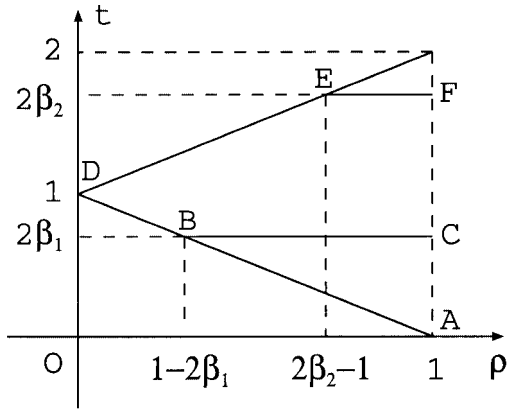

Fig. 11. Integration area for region II when $\beta < 1$. The area is given by *ABC* if $\beta \leq 1/2$ and by *ADEF* if $1/2 < \beta < 1$.

For $\beta \geq 1$, where II is a semicircle [Fig. 2(b)], the range of ρ over which the integration is performed is $|t - 1| \leq \rho \leq 1$; hence

$$q_2(t) = \int_{|t-1|}^{1} \mathrm{d}\rho \, \frac{\rho(1 + t^2 - \rho^2)}{t[-\rho^4 + 2(t^2 + 1)\rho^2 - (t^2 - 1)^2]^{1/2}} = \frac{\sqrt{4 - t^2}}{2}, \qquad 0 \leq t \leq 2. \tag{A3}$$

In the second case, where $\beta < 1$ [Fig. 2(a)], the integration is over

$$\begin{aligned} &1 - \rho \leq t \leq 2\beta, && \rho \geq |2\beta - 1|, && \beta < 1, \\ &1 - \rho \leq t \leq 1 + \rho, && \rho < 2\beta - 1, && 1/2 < \beta < 1. \end{aligned} \tag{A4}$$

This integration region [inequalities (A4)] for region II can be simplified to (see Fig. 11)

$$|t - 1| \leq \rho \leq 1, \qquad 0 \leq t \leq 2\beta. \tag{A5}$$

Area density $q_2(t)$ is still given by Eq. (A3) in the second case but with a different constraint of t specified in inequalities (A5).

The area density of region III is given by

$$q_3(t) = \frac{\arccos \beta - \beta \sqrt{1 - \beta^2}}{2} \delta(t - 2\beta), \qquad \beta < 1, \tag{A6}$$

where $\delta(t)$ is the Dirac delta function.

In region IV let us rewrite $\eta = \sin \theta$; we have

$$\begin{aligned} t = 2\sqrt{1 - \sin^2 \theta}; \qquad & 0 \leq \xi \leq \beta + \cos \theta; \\ \pi/2 \leq \theta \leq \pi - \arccos \beta, \quad & \beta < 1; \\ \pi/2 \leq \theta \leq \pi, \quad & \beta \geq 1 \end{aligned} \tag{A7}$$

from Eq. (11). We can solve

$$\sin \theta = \sqrt{1 - t^2/4}. \tag{A8}$$

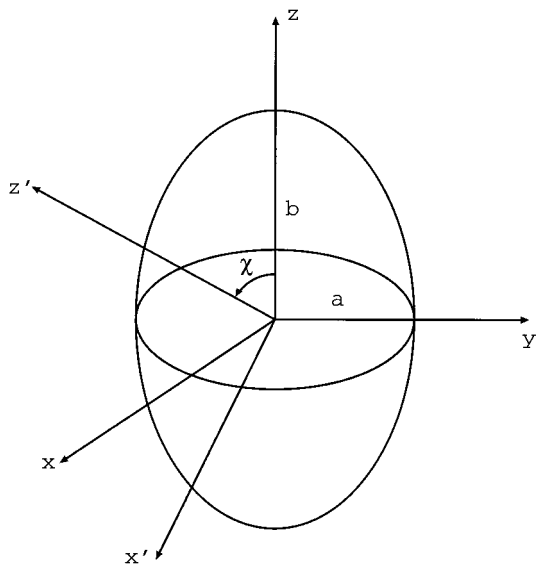

Fig. 12. Spheroid whose revolutional axis makes an angle χ with the incident beam.

Area integration

$$\int \mathrm{d}\xi \mathrm{d}\eta = q_4(t)\mathrm{d}t$$
$$= -(\beta + \cos\theta)\mathrm{d}\sin\theta$$
$$= (t/2)[\beta - (t/2)]\sqrt{4 - t^2}\,\mathrm{d}t \qquad \text{(A9)}$$

gives the area density

$$q_4(t) = \frac{(t/2)[\beta - (t/2)]}{\sqrt{4 - t^2}}, \qquad 0 \le t \le 2\min(\beta, 1). \qquad \text{(A10)}$$

The total area density is thus given by Eq. (12).

Appendix B: Ray Distribution of a Spheroid

Consider a spheroid with semisize b of a revolution axis and axial ratio $\epsilon = a/b$. The incident light forms an angle χ between the revolution axis of the spheroid and the propagation direction of the incident beam. Inside the coordinate system $x'yz'$ whose z' axis coincides with incidence direction $\cos\chi\hat{z} + \sin\chi\hat{x}(0 \le \chi < \pi/2)$ of light (see Fig. 12), the spheroid is bounded by

$$\frac{(x'\cos\chi + z'\sin\chi)^2}{a^2} + \frac{y^2}{a^2} + \frac{(-x'\sin\chi + z'\cos\chi)^2}{b^2} = 1. \qquad \text{(B1)}$$

The geometrical path of a ray passing through $(x', y, 0)$ on the $z' = 0$ plane is given by

$$l = \frac{2ab}{(a^2\cos^2\chi + b^2\sin^2\chi)^{1/2}}[1 - (a^2\cos^2\chi + b^2\sin^2\chi)^{-1}x'^2 - a^{-2}y^2]^{1/2}. \qquad \text{(B2)}$$

The projected area of the spheroid is the area formed by the points of tangency ($l = 0$) on the $z' = 0$ plane, yielding an ellipse with semiaxes $(a^2\cos^2\chi + b^2\sin^2\chi)^{1/2}$ and a. The projection area is given by

$$\Sigma = \pi a(a^2\cos^2\chi + b^2\sin^2\chi)^{1/2}$$
$$= \pi\epsilon b^2(\epsilon^2\cos^2\chi + \sin^2\chi). \qquad \text{(B3)}$$

We rewrite $x' = (a^2\cos^2\chi + b^2\sin^2\chi)^{1/2}\rho\cos\theta$ and $y = a\rho\sin\theta$, where $0 \le \rho \le 1$ and $0 \le \theta \le 2\pi$; the geometrical path [Eq. (B2)] can be written as

$$l = \frac{2ab}{(a^2\cos^2\chi + b^2\sin^2\chi)^{1/2}}(1 - \rho^2)^{1/2}. \qquad \text{(B4)}$$

The area inside projection area Σ that results in a geometrical path within $[l, l + dl)$ is then

$$\mathrm{d}\Sigma = a(a^2\cos^2\chi + b^2\sin^2\chi)^{1/2}\,2\pi\rho\mathrm{d}\rho$$
$$= \frac{\pi(\epsilon^2\cos^2\chi + \sin^2\chi)^{3/2}}{2\epsilon}l\mathrm{d}l. \qquad \text{(B5)}$$

Thus the geometrical path distribution of the rays is given by

$$p^{\mathrm{sph}}(l) = \frac{\mathrm{d}\Sigma}{\Sigma} = \frac{1}{2\epsilon^2 b^2}(\epsilon^2\cos^2\chi + \sin^2\chi)l \times H\left[\frac{2\epsilon b}{(\epsilon^2\cos^2\chi + \sin^2\chi)^{1/2}} - l\right], \qquad l \ge 0. \qquad \text{(B6)}$$

This equation reduces to

$$p^{\mathrm{sph}}(l) = \frac{1}{2b^2}lH(2b - l), \qquad \epsilon = 1 \qquad \text{(B7)}$$

for a sphere ($\epsilon = 1$).

The ray distribution for a system of such spheroids at a fixed orientation χ with a log-normal size distribution [Eq. (32)] for the semisize of its revolutional axis is given by

$$p_{\mathrm{pol}}{}^{\mathrm{sph}}(l) = \frac{(\epsilon^{-2}\sin^2\chi + \cos^2\chi)l}{4} \times \frac{\mathrm{erfc}\{(1/\sqrt{2\sigma})\ln[(\epsilon^{-2}\sin^2\chi + \cos^2\chi)^{1/2}l/(2a_m)]\}}{a_m{}^2\exp(2\sigma^2)} \qquad \text{(B8)}$$

by use of Eq. (4), where $\mathrm{erfc}(x)$ is the complementary error function.

The mean geometrical path and the mean-square geometrical path are given by

$$\langle l\rangle^{\mathrm{sph}} = \frac{4}{3}\frac{\epsilon b}{(\epsilon^2\cos^2\chi + \sin^2\chi)^{1/2}}$$
$$\langle l^2\rangle^{\mathrm{sph}} = \frac{2\epsilon^2 b^2}{\epsilon^2\cos^2\chi + \sin^2\chi} \qquad \text{(B9)}$$

for a spheroid oriented at an angle χ with respect to the incident light.

Table 1. Average Geometrical Cross Sections, Mean and Mean-Squared Geometrical Paths of Spheres, Randomly Oriented Spheroids, and Finite Circular Cylinders

Property	Sphere	Spheroid with a Semisize of Revolution b, $\epsilon = a/b$		Finite Cylinder ($\epsilon = e^{-1} = 2a/L$)
$\langle\Sigma\rangle_{\mathrm{rn}}$	πa^2	$\frac{\pi}{2}\epsilon^2 b^2 + \frac{\pi}{2}\epsilon b^2(1-\epsilon^2)^{-1/2}\arcsin\sqrt{1-\epsilon^2}$	$\epsilon \le 1$	$\frac{\pi}{2}a^2(2e+1)$
		$\frac{\pi}{2}\epsilon^2 b^2 + \frac{\pi}{2}\epsilon b^2(\epsilon^2-1)^{-1/2}\ln(\epsilon+\sqrt{\epsilon^2-1})$	$\epsilon > 1$	
$\langle l\rangle_{\mathrm{rn}}$	$\frac{4}{3}a$	$\frac{8\epsilon/3}{\epsilon+(1-\epsilon^2)^{-1/2}\arcsin\sqrt{1-\epsilon^2}}b$	$\epsilon \le 1$	$\frac{2a}{1+a/L}$
		$\frac{8\epsilon/3}{\epsilon+(\epsilon^2-1)^{-1/2}\ln(\epsilon+\sqrt{\epsilon^2-1})}b$	$\epsilon > 1$	
$\sqrt{\langle l^2\rangle_{\mathrm{rn}}}$	$2a$	$\left(\frac{\arcsin\sqrt{1-\epsilon^2}}{\epsilon\sqrt{1-\epsilon^2}+\arcsin\sqrt{1-\epsilon^2}}\right)^{1/2}2\epsilon b$	$\epsilon \le 1$	$\sqrt{\text{Eq. (38)}}$
		$\left[\frac{\ln(\epsilon+\sqrt{\epsilon^2-1})}{\epsilon\sqrt{\epsilon^2-1}+\ln(\epsilon+\sqrt{\epsilon^2-1})}\right]^{1/2}2\epsilon b$	$\epsilon > 1$	

Appendix C. Geometrical Cross Sections, Mean and Mean-Square-Root Paths of Spheres, and Randomly Oriented Spheroids and Cylinders

Table 1 lists the average geometrical cross sections, the mean and the mean-square-root geometrical paths for a sphere of radius a, a randomly oriented spheroid with revolutional semiaxis b and aspect ratio $\epsilon = a/b$, and a randomly oriented finite circular cylinder with height L and radius a.

The author is grateful for the support of the U.S. Department of the Army (grant DAMD17-02-1-0516). The U.S. Army Medical Research Acquisition Activity is the awarding and administering acquisition office. This research is also supported in part by NASA. The author is indebted to the anonymous reviewers whose constructive comments helped to improve the first version of this paper.

References

1. H. C. van de Hulst, *Light Scattering by Small Particles* (Dover, New York, 1981).
2. M. I. Mishchenko, J. W. Hovenier, and L. D. Travis, eds., *Light Scattering by Nonspherical Particles: Theory, Measurements, and Applications* (Academic, San Diego, Calif., 1999).
3. E. M. Purcell and C. R. Pennypacker, "Scattering and absorption of light by nonspherical dielectric grains," Astrophys. J. **186,** 705–714 (1973).
4. B. T. Draine and P. J. Flatau, "Discrete-dipole approximation for scattering calculations," J. Opt. Soc. Am. A **11,** 1491–1499 (1994).
5. M. I. Mishchenko and L. D. Travis, "Capabilities and limitations of a current FORTRAN implementation of the T-matrix method for randomly oriented, rotationally symmetric scatterers," J. Quant. Spectrosc. Radiat. Transfer **60,** 309–324 (1998).
6. S. A. Ackerman and G. L. Stephens, "The absorption of solar radiation by cloud droplets: an application of anomalous diffraction theory," J. Atmos. Sci. **44,** 1574–1588 (1987).
7. W. A. Farone and M. J. I. Robinson, "The range of validity of the anomalous diffraction approximation to electromagnetic scattering by a sphere," Appl. Opt. **7,** 643–645 (1968).
8. S. Asano and M. Sato, "Light scattering by randomly oriented spheroidal particles," Appl. Opt. **19,** 962–974 (1980).
9. A. Maslowska, P. J. Flatau, and G. L. Stephens, "On the validity of the anomalous diffraction theory to light scattering by cubes," Opt. Commun. **107,** 35–40 (1994).
10. Y. Liu, W. P. Arnott, and J. Hallett, "Anomalous diffraction theory for arbitrarily oriented finite circular cylinders and comparison with exact T-matrix results," Appl. Opt. **37,** 5019–5030 (1998).
11. A. J. Baran, J. S. Foot, and D. L. Mitchell, "Ice-crystal absorption: a comparison between theory and implications for remote sensing," Appl. Opt. **37,** 2207–2215 (1998).
12. F. D. Bryant and P. Latimer, "Optical efficiencies of large particles of arbitrary shape and orientation," J. Colloid Interface Sci. **30,** 291–304 (1969).
13. P. Latimer, "Light scattering by ellipsoids," J. Colloid Interface Sci. **53,** 102–109 (1975).
14. D. A. Cross and P. Latimer, "General solutions for the extinction and absorption efficiencies of arbitrarily oriented cylinder by anomalous-diffraction methods," J. Opt. Soc. Am. **60,** 904–907 (1970).
15. P. Chýlek and J. D. Klett, "Extinction cross sections of nonspherical particles in the anomalous diffraction approximation," J. Opt. Soc. Am. A **8,** 274–281 (1991).
16. M. Xu, M. Lax, and R. R. Alfano, "Light anomalous diffraction using geometrical path statistics of rays and Gaussian ray approximation," Opt. Lett. **28,** 179–181 (2003).
17. A. Katz, A. Alimova, M. Xu, E. Rudolph, M. Shah, H. Savage, R. Rosen, S. A. McCormick, and R. R. Alfano, "Bacteria size determination by elastic light scattering," IEEE J. Sel. Top. Quantum Electron. 9 (to be published).
18. A. A. Kokhanovsky, *Optics of Light Scattering Media: Problems and Solutions* (Wiley, New York, 1999).